SIAM J. NUMER. ANAL.
Vol. 59, No. 3, pp. 1195–1217

TAYLOR–HOOD DISCRETIZATION OF THE REISSNER–MINDLIN PLATE*

DIETMAR GALLISTL† AND MIRA SCHEDENSACK‡

Abstract. A shear-locking free finite element discretization of the Reissner–Mindlin plate model is introduced. The rotation is discretized with piecewise polynomials of degree $k+2$ while the degree $k \geq 0$ is used for the displacement gradient. The method is closely related to the (generalized) Taylor–Hood pairing. In this case the general theory of saddle-point problems with penalty cannot exclude that the convergence speed for the rotation is limited by the lower rate expected for the displacement. However, in this paper, it is shown that the rotations are approximated at optimal order of accuracy. This superconvergence phenomenon is proved by means of the approximation properties of the Fortin operator for the Taylor–Hood element and the Galerkin projection.

Key words. Reissner–Mindlin, mixed finite element, superconvergence, Taylor–Hood

AMS subject classifications. 65N12, 65N15, 65N30, 74K20

DOI. 10.1137/20M1343397

1. Introduction.

The Reissner–Mindlin model is a classical description for the elastic response of a moderately thick plate whose mid-surface Ω is a subset of the xy plane subject to some load in z direction. More precisely, let $\Omega \subseteq \mathbb{R}^2$ be a simply connected, open, and polygonal Lipschitz domain. Given the plate's thickness $t > 0$ and a scalar function $f \in L^2(\Omega)$ representing the vertical force, the vertical displacement $w \in H^1_0(\Omega)$ and the rotation vector $\phi \in \Phi := [H^1_0(\Omega)]^2$ are the solution to the following variational problem,

$$a(\phi,\psi) + t^{-2}(\nabla w - \phi, \nabla v - \psi)_{L^2(\Omega)} = (f, v)_{L^2(\Omega)} \quad \text{for all } (v,\psi) \in H^1_0(\Omega) \times \Phi. \tag{1.1}$$

Here, $a(\cdot,\cdot)$ is a coercive and continuous bilinear form on Φ, and the thickness t is rescaled by certain material constants (details in section 2). The phenomenon that low-order finite element methods (FEMs) behave poorly for this model when t is small compared to the mesh size, is known as shear locking. There is a vast literature on the numerical approximation of (1.1), and we refer to [11, 9] and the references therein for an overview. Since [10], the error analysis is usually based on the shear variable

$$\zeta := t^{-2}(\nabla w - \phi) \tag{1.2}$$

and its Helmholtz decomposition

$$\zeta = \nabla r + \operatorname{Curl} p. \tag{1.3}$$

It is well known [9] that (1.1) can be decomposed in a system of simpler equations. Most importantly, (ϕ, p) can be interpreted as a velocity-pressure pair in a Stokes

*Received by the editors June 5, 2020; accepted for publication (in revised form) March 2, 2021; published electronically May 4, 2021.
https://doi.org/10.1137/20M1343397
Funding: The work of the second author was supported by the DFG Priority Program 1748 under the project "Robust and Efficient Finite Element Discretizations for Higher-Order Gradient Formulations" grant SCHE1885/1-1.
†Institut für Mathematik, Universität Jena, 07743 Jena, Germany (dietmar.gallistl@uni-jena.de).
‡Mathematisches Institut, Universität Leipzig, PF 10 09 20, 04009 Leipzig, Germany (mira.schedensack@math.uni-leipzig.de).

system with penalty term. The method by [5] was the first to mimic this equivalence on the finite element level with pointwise relations, namely, with a discrete Helmholtz decomposition. Therein the variables w, r are discretized with first order (nonconforming) finite elements, and (ϕ, p) is discretized with the Mini (or stabilized $P_1 - P_1$) pair. The recent work [24] formulated a generalization of the discrete Helmholtz decomposition to higher polynomial degrees and thereby established higher-order analogues of the nonconforming P_1 FEM. In view of the original purpose of the discrete Helmholtz decomposition, the results of [24] appear to be an appropriate tool for the numerical analysis of the Reissner–Mindlin plate. With this idea it is possible to modify the original scheme by Arnold and Falk in two respects. The first novelty lies in the possibility to use arbitrary polynomial degrees. Secondly, instead of the Mini element used in [5] we propose the use of the Taylor–Hood pair. Since the singular perturbation in the Stokes-like system involves the Laplacian $t^2\Delta p$, continuous pressure pairs appear as the first choice. For the Stokes problem the polynomial degree is optimally chosen one degree higher for the velocity than for the pressure so that the asymptotic approximation properties are correctly balanced. These $P_{m+1} - P_m$ elements with continuous pressure are known as (generalized) Taylor–Hood elements [8]. In this sense, the stabilized $P_m - P_m$ pairs are somewhat suboptimal. On the other hand, the decomposition (1.3) naturally has its finite element equivalent in a subspace of vector-valued piecewise P_{m-1} polynomials, which requires discrete analoga of (1.2) to involve some degree-lowering projection (or reduced integration) operator. An immediate use of the saddle-point theory with penalty terms therefore predicts that the global H^1 norm of the error in the ϕ variable is bounded from above by the sum of best approximation errors of the involved variables w, r, ϕ in H^1 and p in a t-weighted H^1 norm. Hence, choosing ϕ one degree higher than the other variables does not improve the convergence rate predicted by this error estimate that has a global character with norms involving all unknowns.

In this paper, we prove that the variable ϕ is indeed approximated in a superconvergent way. That is, the seeming loss in accuracy is just an artifact of the too general error analysis. In the setting of [5], for instance, this means that keeping the approximation space for w unchanged and replacing the bubble-enriched P_1 elements by piecewise quadratic vector fields, the approximation of ϕ is in fact improved by one order. This lowest-order case is discussed in section 3 separately. On the one hand, that section illustrates the error analysis without the need of introducing the generalized nonconforming FEM. On the other hand, the result in the lowest-order case is slightly sharper than in the general situation. The convergence analysis is valid under minimal regularity assumptions.

An important aspect of the proposed method is that it is shear-locking free; that is, the constants appearing in the error estimates are robust with respect to small plate thickness t. The only t-dependence in the upper error bound from the main result in Corollary 5.7 lies in the approximability of the solution. This means that no other method with the same approximation spaces can yield better results (up to some t-independent constant). Error estimates in terms of convergence rates naturally contain the norms of derivatives of the exact solution as a factor on the right-hand side. Whether this resulting error estimate is robust in the thickness t will depend on the regularity of the exact solution. However, the refined error estimate states quasi-optimality and is thus superior to asymptotic estimates if, e.g., nonuniform meshes are used to resolve the t-dependent boundary layers and hereby improve the approximation properties of the underlying spaces.

In order to obtain these results, we use tools from mixed finite element theory. Namely, we employ the Fortin operator for the Taylor–Hood element with best-approximation properties. We note that such an operator was constructed by [19] for $m \in \{2, 3\}$ in an explicit design using special quadrature formulas. The approach seems not to generalize easily to $m \geq 4$, and the proof we give in this paper relies on the more general statement that stability automatically implies the existence of a Fortin operator with best-approximation properties. The latter is usually of marginal importance when the Fortin operator is used in a mere stability analysis. Here, however, the property is helpful in a refined error analysis.

The proposed method allows for an easy implementation (see section 4.2). The finite element spaces involved in the implementation are the standard finite element spaces of (generalized) Taylor–Hood finite elements, namely, continuous piecewise polynomials of degree $k + 2$ and continuous piecewise polynomials of degree $k + 1$. The local number of degrees of freedom of the system that has to be solved is 15 for the second-order method ($k = 0$). Compared to other existing second-order methods, this is a low number of degrees of freedom.

The remaining parts of this article are organized as follows: Section 2 provides notation and preliminary results. The method and its error analysis are presented in the lowest-order case in section 3. The discretization with arbitrary polynomial degree $k \geq 0$ is presented in section 4 and a priori error estimates are shown in section 5. The paper is concluded with the computational results in section 6.

Standard notation on Lebesgue and Sobolev spaces applies throughout this paper. The L^2 inner product is denoted by $(v, w)_{L^2(\Omega)}$ and $\|\bullet\| := \|\bullet\|_{L^2(\Omega)}$ denotes the L^2 norm. The H^k seminorm over Ω is denoted by $|\bullet|_k$. The space of $L^2(\Omega)$ functions with vanishing global average reads $L^2_0(\Omega)$. For a function v and a vector field ψ, the following differential operators are defined

$$\operatorname{div} \psi = \partial_1\psi_1 + \partial_2\psi_2, \quad \operatorname{rot}\psi = \partial_1\psi_2 - \partial_2\psi_1, \quad \operatorname{Curl} v = \begin{pmatrix} -\partial_2 v \\ \partial_1 v \end{pmatrix}.$$

The notation $A \lesssim B$ abbreviates $A \leq CB$ for some constant C that is independent of the mesh size and the plate's thickness t.

2. Preliminaries. This section lists notation and a lemma on the Fortin operator.

2.1. Notation. Bilinear forms. The bilinear form a is assumed to be symmetric, coercive, and continuous. This is satisfied for the standard Reissner–Mindlin plate model, namely, $a(\phi, \psi) := (\varepsilon(\phi), \mathbb{C}\varepsilon(\psi))_{L^2(\Omega)}$ for the linear Green strain $\varepsilon(\cdot) = \operatorname{sym} D(\cdot)$ and the linear elasticity tensor $\mathbb{C}$ that acts on any symmetric matrix $A \in \mathbb{R}^{2\times 2}$ as follows:

$$\mathbb{C}A = \frac{E}{12(1-\nu^2)}((1-\nu)A + \nu \operatorname{tr}(A) I_{2\times 2}).$$

For isotropic materials it is determined by Young's modulus $E > 0$ and the Poisson ratio $0 < \nu < 1/2$. The parameter t is defined by $t := \lambda^{-1/2}\tilde{t}$ with the plate thickness $\tilde{t}$ and the constant $\lambda = (1+\nu)^{-1}E\kappa/2$ with a shear correction factor κ usually chosen as $5/6$. More details on the mathematical model can be found in [8, 9].

The scalar product a induces a norm $\|\!|\bullet|\!\| := \sqrt{a(\bullet,\bullet)}$ on Φ, which is equivalent to the H^1 seminorm. For convenient reading we write

$$b(\psi, q) := (\psi, \operatorname{Curl} q)_{L^2(\Omega)} \quad \text{for any } (\psi, q) \in \Phi \times Q$$

with $Q := H^1(\Omega) \cap L^2_0(\Omega)$ and note that integration by parts implies the continuity

$$b(\psi, q) \leq |\psi|_1 \, \|q\| \quad \text{for any } (\psi, q) \in \Phi \times Q. \tag{2.1}$$

Define furthermore the H^1 inner product $c : Q \times Q \to \mathbb{R}$ by

$$c(v, w) := (\operatorname{Curl} v, \operatorname{Curl} w)_{L^2(\Omega)} \quad \text{for any } v, w \in Q,$$

and note that $c(v, v) = |v|_1^2$.

Triangulations. Let $\mathcal{T}$ be a shape-regular triangulation of Ω consisting of at least three triangles. The space of piecewise polynomials of total degree not larger than k is denoted by $P_k(\mathcal{T})$. Define the spaces

$$S^k(\mathcal{T}) := P_k(\mathcal{T}) \cap H^1(\Omega) \text{ and } S^k_0(\mathcal{T}) := P_k(\mathcal{T}) \cap H^1_0(\Omega).$$

Furthermore, let $\Pi_k : L^2(\Omega) \to P_k(\mathcal{T})$ denote the L^2 projection onto $P_k(\mathcal{T})$. The same symbol is used for the component-wise L^2 projection of vector-valued functions. The mesh size $h_{\mathcal{T}} \in P_0(\mathcal{T})$ is defined by $h_{\mathcal{T}}|_T = \operatorname{diam}(T)$ for any $T \in \mathcal{T}$, and $h := \max h_{\mathcal{T}}$.

Elliptic regularity. Let $0 < s \leq 1$ denote the elliptic regularity constant from the Poisson–Neumann problem, i.e., such that for all solutions $z \in H^1(\Omega) \cap L^2_0(\Omega)$ of the Poisson problem with homogeneous Neumann data and right-hand side $f \in L^2(\Omega)$, it holds that

$$\|z\|_{H^{1+s}(\Omega)} \lesssim \|f\|. \tag{2.2}$$

For general Lipschitz polygons, $1/2 < s$ and $s = 1$ on convex domains [22, Thm. 2.4.3].

2.2. Fortin operator. This section briefly shows that discrete stability is enough to conclude the existence of a Fortin operator that in addition has near best-approximation properties. The case relevant to this work is the two-dimensional Taylor–Hood pairing, where the velocities are piecewise polynomials of degree $k + 2 \geq 2$ and the pressures consist of continuous piecewise polynomials of degree $k + 1$.

LEMMA 2.1 (Fortin operator with approximation property). *Let $V_h \subseteq [H^1_0(\Omega)]^2$ and $M_h \subseteq L^2_0(\Omega)$ be closed subspaces satisfying the stability condition*

$$\inf_{q_h \in M_h \setminus \{0\}} \sup_{v_h \in V_h \setminus \{0\}} \frac{(\operatorname{rot} v_h, q_h)_{L^2(\Omega)}}{|v_h|_1 \|q_h\|} \geq \beta > 0.$$

Then there exists a linear operator $\Pi_F : [H^1_0(\Omega)]^2 \to V_h$ such that

$$(\operatorname{rot}(v - \Pi_F v), q_h)_{L^2(\Omega)} = 0 \quad \textit{for all } v \in [H^1_0(\Omega)]^2 \textit{ and all } q_h \in M_h$$

and

$$|v - \Pi_F v|_1 \leq (1 + 2\beta^{-1}) \inf_{v_h \in V_h} |v - v_h|_1.$$

Proof. Given any $v \in [H^1_0(\Omega)]^2$, let $v_h \in V_h$ be its best approximation. Consider the discrete saddle-point problem of finding $(\lambda_h, \mu_h) \in V_h \times M_h$ such that, for all $(w_h, q_h) \in V_h \times M_h$,

$$\begin{aligned}(D\lambda_h, Dw_h)_{L^2(\Omega)} + (\mathrm{rot} w_h, \mu_h)_{L^2(\Omega)} &= 0,\\ (\mathrm{rot}\,\lambda_h, q_h)_{L^2(\Omega)} &= (\mathrm{rot}(v - v_h), q_h)_{L^2(\Omega)},\end{aligned}$$

where D denotes the derivative of a vector valued function. If follows from the assumed inf-sup condition and the classical saddle-point theory [8, Theorem 4.2.3] that this system is uniquely solvable and satisfies the stability $|\lambda_h|_1 \le 2\beta^{-1}\|\mathrm{rot}(v - v_h)\|$. Define $\Pi_F v := v_h + \lambda_h$. This definition and the second equation of the saddle-point system show for any $q_h \in M_h$ that

$$(\mathrm{rot}\Pi_F v, q_h)_{L^2(\Omega)} = (\mathrm{rot} v_h, q_h)_{L^2(\Omega)} + (\mathrm{rot}\lambda_h, q_h)_{L^2(\Omega)} = (\mathrm{rot} v, q_h)_{L^2(\Omega)},$$

which implies the claimed Fortin property. The triangle inequality and the above bound for $|\lambda_h|_1$ show

$$|v - \Pi_F v|_1 \le |v - v_h|_1 + |\lambda_h|_1 \le (1 + 2\beta^{-1})|v - v_h|_1.$$

Since v_h is the best approximation, this implies the asserted approximation property. ∎

3. The lowest order case: The Crouzeix–Raviart–Taylor–Hood discretization. Before we define and analyze the method for arbitrary polynomial degree in sections 4–5 below, this section discusses the lowest-order case. Although this is a special case of the general situation discussed below, the main mathematical arguments are best illustrated in the less technical low-order case. Moreover, the results of Theorem 3.1 are slightly sharper in this situation.

The nonconforming Crouzeix–Raviart finite element space is defined as

$$\begin{aligned}\mathrm{CR}^1_0(\mathcal{T}) := \{v_{\mathrm{CR}} \in P_1(\mathcal{T}) \mid\ & v_{\mathrm{CR}} \text{ is continuous in the midpoints of interior}\\ & \text{edges and vanishes in the midpoints of boundary edges}\}.\end{aligned}$$

Note that $\mathrm{CR}^1_0(\mathcal{T}) \not\subseteq H^1_0(\Omega)$ for nontrivial triangulations. However, the piecewise gradient exists and is denoted by ∇_{NC}. Define $\Phi_h := [S^2_0(\mathcal{T})]^2$. The discretization of (1.1) then seeks $(w_{\mathrm{CR}}, \phi_h) \in \mathrm{CR}^1_0(\mathcal{T}) \times \Phi_h$ with

$$a(\phi_h, \psi_h) + t^{-2}(\nabla_{\mathrm{NC}} w_{\mathrm{CR}} - \Pi_0\phi_h, \nabla_{\mathrm{NC}} v_{\mathrm{CR}} - \Pi_0\psi_h)_{L^2(\Omega)} = (f, v_{\mathrm{CR}})_{L^2(\Omega)} \tag{3.1}$$

for all $(v_{\mathrm{CR}}, \psi_h) \in \mathrm{CR}^1_0(\mathcal{T}) \times \Phi_h$. This discretization coincides with that of [5] except for the discretization space of the rotation. While in the discretization (3.1) the rotation is approximated in $[S^2_0(\mathcal{T})]^2$, in [5] the rotation is discretized with $[S^1_0(\mathcal{T})]^2$ functions enriched by volume bubbles. In their analysis via a mixed system, it seems natural to choose the same approximation order as $\mathrm{CR}^1_0(\mathcal{T})$. However, in Theorem 3.1 below it turns out that one can indeed recover the optimal approximation order for the rotation.

As in [5] the proof of the error estimate of Theorem 3.1 relies on the equivalence of problem (3.1) with a mixed system. The continuous problem (1.1) is equivalent to the following mixed system [10]: Seek $(r, \phi, p, w) \in H^1_0(\Omega) \times \Phi \times Q \times H^1_0(\Omega)$ such that, for all $(s, \psi, q, v) \in H^1_0(\Omega) \times \Phi \times Q \times H^1_0(\Omega)$,

$$(\nabla r, \nabla s)_{L^2(\Omega)} = (f, s)_{L^2(\Omega)} \tag{3.2a}$$

$$a(\phi, \psi) - b(\psi, p) - (\nabla r, \psi)_{L^2(\Omega)} = 0 \tag{3.2b}$$

$$-b(\phi, q) - t^2 c(p, q) = 0 \tag{3.2c}$$

$$(\nabla w, \nabla v)_{L^2(\Omega)} - (\phi, \nabla v)_{L^2(\Omega)} = t^2 (f, v)_{L^2(\Omega)}. \tag{3.2d}$$

Analogously, with the space $Q_h := S^1(\mathcal{T}) \cap L^2_0(\Omega)$, the discrete problem (3.1) can be reformulated as a mixed system: Seek $(r_{\mathrm{CR}}, \phi_h, p_h, w_{\mathrm{CR}}) \in \mathrm{CR}^1_0(\mathcal{T}) \times \Phi_h \times Q_h \times \mathrm{CR}^1_0(\mathcal{T})$ such that, for all $(s_{\mathrm{CR}}, \psi_h, q_h, v_{\mathrm{CR}}) \in \mathrm{CR}^1_0(\mathcal{T}) \times \Phi_h \times Q_h \times \mathrm{CR}^1_0(\mathcal{T})$,

$$(\nabla_{\mathrm{NC}} r_{\mathrm{CR}}, \nabla_{\mathrm{NC}} s_{\mathrm{CR}})_{L^2(\Omega)} = (f, s_{\mathrm{CR}})_{L^2(\Omega)} \tag{3.3a}$$

$$a(\phi_h, \psi_h) - b(\psi_h, p_h) - (\nabla_{\mathrm{NC}} r_{\mathrm{CR}}, \psi_h)_{L^2(\Omega)} = 0 \tag{3.3b}$$

$$-b(\phi_h, q_h) - t^2 c(p_h, q_h) = 0 \tag{3.3c}$$

$$(\nabla_{\mathrm{NC}} w_{\mathrm{CR}}, \nabla_{\mathrm{NC}} v_{\mathrm{CR}})_{L^2(\Omega)} - (\phi_h, \nabla_{\mathrm{NC}} v_{\mathrm{CR}})_{L^2(\Omega)} = t^2 (f, v_{\mathrm{CR}})_{L^2(\Omega)}. \tag{3.3d}$$

The proof of the equivalence follows as in [5], the only difference being that Φ_h and Q_h form the inf-sup stable Taylor–Hood pair instead of the Mini element.

The following theorem proves two error estimates that both yield the optimal approximation order. The first error estimate is valid for general right-hand sides $f \in L^2(\Omega)$, and the upper bound involves terms from (3.2), while the second part should be seen as an illustration of Theorem 5.5 below in the case of the lowest polynomial degrees. In that part we assume, for the purpose of illustration, that f is piecewise constant with respect to some possibly coarser triangulation $\mathcal{T}_H$. Then it is known [9] that f can be represented as the divergence of an element of the Raviart–Thomas space, which is defined as

$$\begin{aligned}\mathrm{RT}_0(\mathcal{T}_H) := \{q_{\mathrm{RT}} \in H(\mathrm{div}, \Omega) \mid \text{for all } T \in \mathcal{T}_H \ \exists (a_T, b_T) \in \mathbb{R}^2 \times \mathbb{R} \\ \text{such that for all } x \in T,\ q_{\mathrm{RT}}|_T(x) = a_T + b_T x\},\end{aligned}$$

so that $f = -\operatorname{div} \eta$ for some $\eta \in \mathrm{RT}_0(\mathcal{T}_H)$. Since $-\operatorname{div} \nabla r = f = -\operatorname{div} \eta$, the field η admits a decomposition

$$\eta = \nabla r + \mathrm{Curl}\, \gamma \tag{3.4}$$

with some $\gamma \in H^1(\Omega) \cap L^2_0(\Omega)$. Recall the elliptic regularity constant s from (2.2) of the Poisson–Neumann problem and the maximum mesh size $h = \max h_{\mathcal{T}}$.

THEOREM 3.1. *The discrete solution* $(w_{\mathrm{CR}}, \phi_h) \in \mathrm{CR}^1_0(\mathcal{T}) \times \Phi_h$ *to* (3.1) *and the solution* $(w, \phi) \in H^1_0(\Omega) \times \Phi$ *to* (1.1) *satisfy*

$$\begin{aligned}|\!|\!| \phi - \phi_h |\!|\!| \lesssim \inf_{\varphi_h \in \Phi_h} |\!|\!| \phi - \varphi_h |\!|\!| + h^s \inf_{q_h \in Q_h} |p - q_h|_1 \\ + h^s \inf_{v_{\mathrm{CR}} \in \mathrm{CR}^1_0(\mathcal{T})} \|\nabla_{\mathrm{NC}}(r - v_{\mathrm{CR}})\| + h^s \mathrm{osc}(f, \mathcal{T}),\end{aligned}$$

where p *is as in* (3.2) *and* $\mathrm{osc}(f, \mathcal{T}) := \|h_{\mathcal{T}}(f - \Pi_0 f)\|$ *denotes the oscillations of* f. *If there exists a coarse shape-regular triangulation* $\mathcal{T}_H$ *of* Ω *such that* $f \in P_0(\mathcal{T}_H)$ *and* $\mathcal{T}$ *is a refinement of* $\mathcal{T}_H$, *then*

$$|\!|\!| \phi - \phi_h |\!|\!| \lesssim \inf_{\varphi_h \in \Phi_h} |\!|\!| \phi - \varphi_h |\!|\!| + h^s \inf_{q_h \in Q_h} |p - q_h|_1 + h^s \inf_{\delta_h \in Q_h} |\gamma - \delta_h|_1 + \|h^2_{\mathcal{T}} f\|$$

with $\gamma \in H^1(\Omega)$ *from the decomposition* (3.4) *of any given Raviart–Thomas field* $\eta \in \mathrm{RT}_0(\mathcal{T}_H)$ *with* $-\operatorname{div} \eta = f$.

Remark 3.2. The oscillations of f in Theorem 3.1 can be avoided if the right-hand side $(f, v_{\mathrm{CR}})_{L^2(\Omega)}$ in (3.1) is replaced by $(f, Ev_{\mathrm{CR}})_{L^2(\Omega)}$ with a smoothing operator $E : \mathrm{CR}_0^1(\mathcal{T}) \to H_0^1(\Omega)$ as in [25]. This smoothing operator then also appears on the right-hand side of the equivalent mixed system in (3.3a) and (3.3d).

Proof of Theorem 3.1. The proof is split into three steps.

Step 1. This step proves an error estimate that is used for both of the error estimates of Theorem 3.1. Let $\psi_h := \Pi_F \phi \in \Phi_h$ be the Fortin interpolation of ϕ from Lemma 2.1, which exists due to the stability results from [7, 8] and in particular satisfies

$$b(\phi - \psi_h, s_h) = 0 \qquad \text{for all } s_h \in Q_h. \tag{3.5}$$

We start with the obvious decomposition

$$|||\phi - \phi_h|||^2 = a(\phi - \phi_h, \phi - \psi_h) + a(\phi - \phi_h, \psi_h - \phi_h). \tag{3.6}$$

The continuity of a shows for the first term on the right-hand side that

$$a(\phi - \phi_h, \phi - \psi_h) \leq |||\phi - \phi_h||| \, |||\phi - \psi_h|||. \tag{3.7}$$

For the second term of (3.6), the continuous and discrete equation (3.2b) and (3.3b) show

$$a(\phi - \phi_h, \psi_h - \phi_h) = (\nabla r - \nabla_{\mathrm{NC}} r_{\mathrm{CR}}, \psi_h - \phi_h)_{L^2(\Omega)} + b(\psi_h - \phi_h, p - p_h). \tag{3.8}$$

Let $q_h \in Q_h$ be the Galerkin projection of p; i.e., let q_h solve

$$c(q_h, s_h) = c(p, s_h) \qquad \text{for all } s_h \in Q_h.$$

Elementary algebraic manipulations show that the second term of (3.8) equals

$$\begin{aligned} b(\psi_h - \phi_h, p - p_h) = {} & b(\psi_h - \phi, p - p_h) + b(\phi - \phi_h, p - q_h) \\ & - b(\phi - \phi_h, p_h - q_h). \end{aligned} \tag{3.9}$$

The Fortin interpolation property (3.5) and estimate (2.1) lead for the first term on the right-hand side of (3.9) to

$$b(\psi_h - \phi, p - p_h) = b(\psi_h - \phi, p - q_h) \leq |\phi - \psi_h|_1 \, \|p - q_h\|.$$

The second term of (3.9) can be estimated with (2.1) as

$$b(\phi - \phi_h, p - q_h) \leq |\phi - \phi_h|_1 \, \|p - q_h\|.$$

The continuous and discrete problem (3.2c) and (3.3c) and the fact that q_h is the Galerkin projection of p with respect to the scalar product c show that the last term of (3.9) equals

$$\begin{aligned} -b(\phi - \phi_h, p_h - q_h) &= t^2 c(p - p_h, p_h - q_h) \\ &= t^2 c(q_h - p_h, p_h - q_h) = -t^2 |p_h - q_h|_1^2. \end{aligned}$$

The quantity on the right-hand side is nonpositive. Thus,

$$-b(\phi - \phi_h, p_h - q_h) \leq 0.$$

The combination of the foregoing formulae with (3.9) yields

$$b(\psi_h-\phi_h,p-p_h)\le\|p-q_h\|\,(|\phi-\psi_h|_1+|\phi-\phi_h|_1). \tag{3.10}$$

The definition of q_h as the Galerkin projection of p implies that the standard duality technique for the estimate of the L^2 error for the Neumann problem applies and proves

$$\|p-q_h\|\lesssim h^s|p-q_h|_1$$

for the constant s from the elliptic regularity (2.2), only dependent on the geometry of Ω. Furthermore, Céa's lemma proves

$$|p-q_h|_1\le\inf_{s_h\in Q_h}|p-s_h|_1.$$

The quasi-best-approximation property from the Fortin interpolation from Lemma 2.1 and the norm equivalence of $|\!|\!|\bullet|\!|\!|$ and $|\bullet|_1$ prove

$$|\!|\!|\phi-\psi_h|\!|\!|\lesssim\inf_{\varphi_h\in\Phi_h}|\!|\!|\phi-\varphi_h|\!|\!|. \tag{3.11}$$

The combination of the foregoing displayed formulae with (3.6)–(3.8) and (3.10) and the use of the weighted Young inequality and $|\bullet|_1\lesssim|\!|\!|\bullet|\!|\!|$ to absorb $|\phi-\phi_h|_1$ proves

$$\begin{aligned}|\!|\!|\phi-\phi_h|\!|\!|^2\lesssim{}&\inf_{\varphi_h\in\Phi_h}|\!|\!|\phi-\varphi_h|\!|\!|^2+h^{2s}\inf_{s_h\in Q_h}|p-s_h|_1^2\\&+(\nabla r-\nabla_{\mathrm{NC}}r_{\mathrm{CR}},\psi_h-\phi_h)_{L^2(\Omega)}.\end{aligned} \tag{3.12}$$

Step 2. This step proves the first error estimate in Theorem 3.1. Similar to medius analysis techniques [23], the last term on the left-hand side of (3.12) can be estimated as follows. A piecewise integration by parts proves

$$\begin{aligned}&(\nabla_{\mathrm{NC}}(r-r_{\mathrm{CR}}),\psi_h-\phi_h)_{L^2(\Omega)}\\&\quad=-(r-r_{\mathrm{CR}},\mathrm{div}(\psi_h-\phi_h))_{L^2(\Omega)}+\sum_{E\in\mathcal{E}(\Omega)}\int_E[r_{\mathrm{CR}}]_E(\psi_h-\phi_h)\cdot\nu_E\,ds,\end{aligned}$$

where $\mathcal{E}(\Omega)$ denotes the set of interior edges of $\mathcal{T}$, $[\bullet]_E$ denotes the jump across E, and ν_E denotes the (oriented) unit normal of E. Since the jump vanishes in the midpoints of the edges, this can be estimated through a Poincaré inequality on the edges by some constant times

$$\|r-r_{\mathrm{CR}}\|\,|\psi_h-\phi_h|_1+\sum_{E\in\mathcal{E}(\Omega)}h_E\,\|[r_{\mathrm{CR}}]_E\|_{L^2(E)}\,\|\nabla(\psi_h-\phi_h)\|_{L^2(E)}$$

with the length of E denoted by h_E. It is well known [13] that duality arguments for the Crouzeix–Raviart discretization of the Dirichlet–Laplacian lead to the L^2 error estimate

$$\|r-r_{\mathrm{CR}}\|\lesssim h^s\|\nabla_{\mathrm{NC}}(r-r_{\mathrm{CR}})\|$$

(with the same number s for the pure Dirichlet problem, see [22, Thm. 2.4.3]). The Cauchy inequality shows that

$$\begin{aligned}&\sum_{E\in\mathcal{E}(\Omega)}h_E\,\|[r_{\mathrm{CR}}]_E\|_{L^2(E)}\,\|\nabla(\psi_h-\phi_h)\|_{L^2(E)}\\&\quad\le\sqrt{\sum_{E\in\mathcal{E}(\Omega)}h_E\,\|[r_{\mathrm{CR}}]_E\|_{L^2(E)}^2}\sqrt{\sum_{E\in\mathcal{E}(\Omega)}h_E\,\|\nabla(\psi_h-\phi_h)\|_{L^2(E)}^2}.\end{aligned} \tag{3.13}$$

Standard efficiency error estimates of nonconformity residuals [17, 26] show that the first term on the right-hand side of (3.13) is controlled by $h\|\nabla_{\mathrm{NC}}(r-r_{\mathrm{CR}})\|$, while trace and inverse estimates show that the second term of (3.13) is controlled by $|\psi_h-\phi_h|_1$. This and the combination of the above displayed formulae leads to

$$(\nabla_{\mathrm{NC}}(r-r_{\mathrm{CR}}),\psi_h-\phi_h)_{L^2(\Omega)}\lesssim h^s\|\nabla_{\mathrm{NC}}(r-r_{\mathrm{CR}})\|\,|\psi_h-\phi_h|_1.$$

The analysis of [23, 14] proves the near best-approximation property

$$\|\nabla_{\mathrm{NC}}(r-r_{\mathrm{CR}})\|\lesssim\inf_{v_{\mathrm{CR}}\in\mathrm{CR}^1_0(\mathcal{T})}\|\nabla_{\mathrm{NC}}(r-v_{\mathrm{CR}})\|+\mathrm{osc}(f,\mathcal{T}).$$

With the norm bound $|\cdot|_1\lesssim|\!|\!|\cdot|\!|\!|$ plus the triangle and weighted Young inequalities we thus deduce for any $\varepsilon>0$ that

$$\begin{aligned}(\nabla_{\mathrm{NC}}(r-r_{\mathrm{CR}}),\psi_h-\phi_h)_{L^2(\Omega)}\lesssim\frac{1}{2\varepsilon}h^{2s}\left(\inf_{v_{\mathrm{CR}}\in\mathrm{CR}^1_0(\mathcal{T})}\|\nabla_{\mathrm{NC}}(r-v_{\mathrm{CR}})\|+\mathrm{osc}(f,\mathcal{T})\right)^2\\+\varepsilon|\!|\!|\phi-\psi_h|\!|\!|^2+\varepsilon|\!|\!|\phi-\phi_h|\!|\!|^2.\end{aligned}$$

Inserting this expression in (3.12) and absorbing the term involving $\phi-\phi_h$ (for sufficiently small ε) yields the first error estimate of Theorem 3.1 (because $\phi-\psi_h$ is quasi-optimal by (3.11)).

Step 3. This step proves the second error estimate in Theorem 3.1. By assumption $f\in P_0(\mathcal{T}_H)$ and therefore there exists $\eta\in\mathrm{RT}_0(\mathcal{T}_H)$ with $-\operatorname{div}\eta=f$ pointwise. Furthermore, a computation of the divergence for a Raviart–Thomas function shows that for all $T\in\mathcal{T}$

$$\eta|_T(x)=\Pi_0\eta-\frac{1}{2}\,f|_T\cdot(x-\mathrm{mid}(T)) \tag{3.14}$$

for the barycenter $\mathrm{mid}(T)$ of T. Since $-\operatorname{div}\eta=f=-\operatorname{div}\nabla r$, the Helmholtz decomposition [9] implies (3.4). Since the normal component of η is constant along any edge of $\mathcal{T}$ and the jump of Crouzeix–Raviart functions vanishes in the midpoints of edges, a piecewise integration by parts reveals that

$$(\nabla_{\mathrm{NC}}v_{\mathrm{CR}},\eta)_{L^2(\Omega)}=(v_{\mathrm{CR}},-\operatorname{div}\eta)_{L^2(\Omega)}\qquad\text{for all } v_{\mathrm{CR}}\in\mathrm{CR}^1_0(\mathcal{T}).$$

Therefore

$$(\nabla_{\mathrm{NC}}r_{\mathrm{CR}},\nabla_{\mathrm{NC}}v_{\mathrm{CR}})_{L^2(\Omega)}=(f,v_{\mathrm{CR}})_{L^2(\Omega)}=(\eta,\nabla_{\mathrm{NC}}v_{\mathrm{CR}})_{L^2(\Omega)}.$$

This and the discrete Helmholtz decomposition of [5] imply

$$\Pi_0\eta=\nabla_{\mathrm{NC}}r_{\mathrm{CR}}+\operatorname{Curl}\gamma_h$$

for some $\gamma_h\in S^1(\mathcal{T})\cap L^2_0(\Omega)$. Therefore, the last term of (3.12) reads

$$(\nabla r-\nabla_{\mathrm{NC}}r_{\mathrm{CR}},\psi_h-\phi_h)_{L^2(\Omega)}=(\eta-\Pi_0\eta,\psi_h-\phi_h)_{L^2(\Omega)}-b(\psi_h-\phi_h,\gamma-\gamma_h). \tag{3.15}$$

The first term on the right-hand side of (3.15) can be estimated with a piecewise Poincaré inequality as

$$\begin{aligned}(\eta-\Pi_0\eta,\psi_h-\phi_h)_{L^2(\Omega)}&=(\eta-\Pi_0\eta,(\psi_h-\phi_h)-\Pi_0(\psi_h-\phi_h))_{L^2(\Omega)}\\&\lesssim\|h_{\mathcal{T}}(\eta-\Pi_0\eta)\|\,|\psi_h-\phi_h|_1.\end{aligned}$$

The formula (3.14) proves

$$\|h_{\mathcal{T}}(\eta - \Pi_0\eta)\| \leq \|h_{\mathcal{T}}^2 f\|.$$

The combination with (3.15) and (2.1) shows

$$(\nabla r - \nabla_{\mathrm{NC}} r_{\mathrm{CR}}, \psi_h - \phi_h)_{L^2(\Omega)} \lesssim |\phi_h - \psi_h|_1(\|h_{\mathcal{T}}^2 f\| + \|\gamma - \gamma_h\|).$$

The discrete and continuous Helmholtz decompositions of η and $\Pi_0\eta$ show the Galerkin orthogonality

$$c(\gamma - \gamma_h, \delta_h) = 0 \qquad \text{for all } \delta_h \in Q_h.$$

Therefore, as above, the L^2 error estimate and Céa's lemma prove

$$\|\gamma - \gamma_h\| \lesssim h^s \inf_{\delta_h \in Q_h} |\gamma - \delta_h|_1.$$

Similar to the final argument in step 2, the combination of the above displayed inequalities with (3.12), (3.11), and a triangle inequality and the absorption of $|||\phi - \phi_h|||$ proves the second error estimate of Theorem 3.1. ∎

Theorem 3.1 covers the regime $h \lesssim t$ and will be generalized to higher polynomial degrees in Theorem 5.5 below. The case $t \lesssim h$ is covered in Proposition 5.1 and Corollary 5.7, which we do not separately state for the lowest-order case.

4. Discretization for arbitrary polynomial degree. This section defines the new discretization for arbitrary $k \geq 0$ in section 4.1. Due to the implicitly defined discretization space Z_h below, the implementation requires Lagrange multipliers. Section 4.2 introduces an equivalent Schur-like system that can be used for the implementation. The error analysis in section 5 below relies on the equivalence of the discretization to a mixed system that is proved in section 4.3. Equivalence here means that the rotation part of the discrete solution of all three formulations is the same.

4.1. Discretization. As in section 3, the discretization of (1.1) involves a nonconforming approximation σ_h of ∇w. The crucial property of the nonconforming space for the error analysis is that it satisfies a Helmholtz decomposition. This is not true for most of the known generalizations of the nonconforming Crouzeix–Raviart FEM to higher polynomial degrees as, e.g., in [20, 16, 2]. We therefore follow [24] and define the nonconforming space via a discrete Helmholtz decomposition. It is important to note that—in contrast to the Crouzeix–Raviart finite element in the lowest-order case—the resulting "discrete gradients" will generally not be piecewise gradients in a pointwise sense. We employ the following discrete spaces for $k \geq 0$,

$$\begin{aligned} \Phi_h &:= [S_0^{k+2}(\mathcal{T})]^2 && \subseteq \Phi, \\ Q_h &:= S^{k+1}(\mathcal{T}) \cap L_0^2(\Omega) && \subseteq Q, \\ X_h &:= [P_k(\mathcal{T})]^2. \end{aligned}$$

Note that Φ_h and Q_h are the stable Taylor–Hood pair [8] for the Stokes system. The Helmholtz decomposition in two dimensions states that the gradients of $H_0^1(\Omega)$ functions are the orthogonal complement of $\operatorname{Curl} Q$, written

$$[L^2(\Omega)]^2 = \nabla H_0^1(\Omega) \oplus \operatorname{Curl} Q. \tag{4.1}$$

This relation was used in [24], where the following space of discrete gradients was introduced:

$$Z_h := \{\sigma_h \in X_h \mid (\sigma_h, \operatorname{Curl} q_h)_{L^2(\Omega)} = 0 \text{ for all } q_h \in Q_h\}.$$

Then the discrete Helmholtz decomposition

$$X_h = Z_h \oplus \operatorname{Curl} Q_h \tag{4.2}$$

follows, as in [24], from the definition of Z_h and $\operatorname{Curl} Q_h \subseteq X_h$. Note that in general $Z_h \not\subseteq \nabla H_0^1(\Omega)$.

The discretization of the Reissner–Mindlin system is as follows. Let $\eta \in H(\operatorname{div}, \Omega)$ be given with $-\operatorname{div} \eta = f$. The discretization of (1.1) seeks $(\sigma_h, \phi_h) \in Z_h \times \Phi_h$ such that for all $(\tau_h, \psi_h) \in Z_h \times \Phi_h$ there holds

$$a(\phi_h, \psi_h) + t^{-2}(\sigma_h - \Pi_k \phi_h, \tau_h - \Pi_k \psi_h)_{L^2(\Omega)} = (\eta, \tau_h)_{L^2(\Omega)}. \tag{4.3}$$

Here, the L^2 projection Π_k plays the role of a reduction or reduced integration operator. This is a positive definite system, and therefore a unique solution exists. The definition of the space Z_h is implicit. An implementation of (4.3) can be based on the Schur complement of the system as explained in section 4.2 below. Note that η can be computed by (numerical) integration of f; in this case $f \in H^m(\Omega)$ implies $\eta \in [H^{m+1}(\Omega)]^2$.

The discrete Helmholtz decomposition of [5] implies that $Z_h = \nabla_{\mathrm{NC}} \mathrm{CR}_0^1(\mathcal{T})$ if $k = 0$. Up to the right-hand side η, the discretization (4.3) therefore equals (3.1) for $k = 0$.

Remark 4.1. The discretization of [5] employs the nonconforming Crouzeix–Raviart space for the approximation of the displacement. Therein, the spaces Φ_h and Q_h are chosen to be the Mini finite element pair [3]. Although at a first glance it seems that the discretization (4.3) with Φ_h from the Taylor–Hood pairing could be suboptimal in ϕ in the asymptotic regime, it turns out in Theorem 5.5 below that the error in ϕ in fact converges with optimal rate.

4.2. Schur complement. This subsection introduces equivalent formulations for (1.1) and (4.3) in (4.4) and (4.7), respectively, that will be used for the error estimate in Proposition 5.1 below. Moreover, in contrast to (4.3), (4.7) is directly accessible for implementation. Consider the problem: Find $(\phi, \alpha) \in \Phi \times Q$ with

$$\begin{aligned} a(\phi, \psi) + b(\psi, \alpha) &= (\eta, \psi)_{L^2(\Omega)} \\ b(\phi, \beta) - t^2 c(\alpha, \beta) &= -t^2 (\eta, \operatorname{Curl} \beta)_{L^2(\Omega)} \end{aligned} \tag{4.4}$$

for all $(\psi, \beta) \in \Phi \times Q$. Note that this is a standard saddle point problem with penalty term [9]. The next result shows the equivalence of (4.4) with (1.1).

Proposition 4.2. *Problems* (1.1) *and* (4.4) *are equivalent in the following sense: If* $(w, \phi) \in H_0^1(\Omega) \times \Phi$ *is the solution to* (1.1)*, then there exists* $\alpha \in Q$ *such that* (ϕ, α) *solves* (4.4)*. On the other hand, if* $(\phi, \alpha) \in \Phi \times Q$ *solves* (4.4)*, then there exists* $w \in H_0^1(\Omega)$ *such that* (w, ϕ) *solves* (1.1)*. Furthermore,* w *and* α *satisfy*

$$\nabla w + t^2 \operatorname{Curl} \alpha = \phi + t^2 \eta, \tag{4.5}$$

and, therefore, the shear force from (1.2) *is given by*

$$\zeta = t^{-2}(\nabla w - \phi) = \eta - \operatorname{Curl} \alpha. \tag{4.6}$$

Proof. Let $(w,\phi)\in H^1_0(\Omega)\times\Phi$ be the solution to (1.1). The definition of η and (1.1) tested with $\psi=0$ proves that ∇w is the $L^2(\Omega)$ projection of $\phi+t^2\eta$ on $\nabla H^1_0(\Omega)$. The Helmholtz decomposition (4.1) then guarantees the existence of $\alpha\in Q$ with (4.5). Note that this equation holds pointwise in $L^2(\Omega)$. This shows for arbitrary $\psi\in\Phi$ that

$$a(\phi,\psi)+(\psi,\operatorname{Curl}\alpha)_{L^2(\Omega)}=a(\phi,\psi)+(\psi,t^{-2}(\phi-\nabla w)+\eta)_{L^2(\Omega)}=(\eta,\psi)_{L^2(\Omega)},$$

where the last equality follows from (1.1). This proves the first equation of (4.4). The definition of α and the $L^2(\Omega)$ orthogonality of $\nabla H^1_0(\Omega)$ and $\operatorname{Curl} Q$ prove for any $\beta\in Q$ that

$$\begin{aligned}(\phi,\operatorname{Curl}\beta)_{L^2(\Omega)}-t^2(\operatorname{Curl}\alpha,\operatorname{Curl}\beta)_{L^2(\Omega)}&=(\nabla w-t^2\eta,\operatorname{Curl}\beta)_{L^2(\Omega)}\\&=-t^2(\eta,\operatorname{Curl}\beta)_{L^2(\Omega)},\end{aligned}$$

which is the second equation of (4.4).

Now let $(\phi,\alpha)\in\Phi\times Q$ solve (4.4). The second equation of (4.4) shows that $\operatorname{Curl}(t^2\alpha)$ is the $L^2(\Omega)$ projection of $t^2\eta+\phi$ onto $\operatorname{Curl} Q$. Hence, by the Helmholtz decomposition (4.1) there exists $w\in H^1_0(\Omega)$ with (4.5). Let $\psi\in\Phi$. Then (4.5) implies

$$a(\phi,\psi)-t^{-2}(\nabla w-\phi,\psi)_{L^2(\Omega)}=a(\phi,\psi)-(\eta-\operatorname{Curl}\alpha,\psi)_{L^2(\Omega)}=0,$$

where the last equation follows from the first equation in (4.4). Given $v\in H^1_0(\Omega)$, the definition of w, the $L^2(\Omega)$ orthogonality of $\nabla H^1_0(\Omega)$ and $\operatorname{Curl} Q$, and $-\operatorname{div}\eta=f$ prove

$$t^{-2}(\nabla w-\phi,\nabla v)_{L^2(\Omega)}=(\eta-\operatorname{Curl}\alpha,\nabla v)_{L^2(\Omega)}=(f,v)_{L^2(\Omega)}.$$

The sum of the two foregoing displayed formulae equals (1.1). The identities (4.5) and (4.6) follow from the above construction. ∎

It is known [7, 8] that the Taylor–Hood element is uniformly inf-sup stable if the mesh consists of at least three triangles. Since (4.4) is a saddle point problem with penalty term [9], the discrete inf-sup condition of the Taylor–Hood pair Φ_h and Q_h for the Stokes problem proves existence and uniqueness of the discrete version of (4.4): Find $(\widetilde{\phi}_h,\alpha_h)\in\Phi_h\times Q_h$ with

$$\begin{aligned}a(\widetilde{\phi}_h,\psi_h)+b(\psi_h,\alpha_h)&=(\Pi_k\eta,\psi_h)_{L^2(\Omega)}\\b(\widetilde{\phi}_h,\beta_h)-t^2c(\alpha_h,\beta_h)&=-t^2(\eta,\operatorname{Curl}\beta_h)_{L^2(\Omega)}\end{aligned}\tag{4.7}$$

for all $(\psi_h,\beta_h)\in\Phi_h\times Q_h$. The following proposition states that this is in fact again equivalent to the discrete problem (4.3).

Proposition 4.3. *Let $(\sigma_h,\phi_h)\in Z_h\times\Phi_h$ be the solution to* (4.3) *and $(\widetilde{\phi}_h,\alpha_h)\in\Phi_h\times Q_h$ be the solution to* (4.7). *Then $\phi_h=\widetilde{\phi}_h$ and*

$$\sigma_h+t^2\operatorname{Curl}\alpha_h=\Pi_k(\phi_h+t^2\eta).\tag{4.8}$$

Proof. The discrete problem (4.3) with $\psi_h=0$ shows that $\sigma_h\in Z_h$ is the $L^2(\Omega)$ projection of $\Pi_k(\phi_h+t^2\eta)$ onto Z_h. The discrete Helmholtz decomposition (4.2) therefore proves that there exists $\hat{\alpha}_h\in Q_h$ with

$$\sigma_h+t^2\operatorname{Curl}\hat{\alpha}_h=\Pi_k(\phi_h+t^2\eta).$$

The discrete problem (4.3) tested with $\psi_h \in \Phi_h$ and $\tau_h = 0$ and this relation lead to

$$\begin{aligned} &a(\phi_h, \psi_h) + b(\psi_h, \hat{\alpha}_h) \\ &\quad = t^{-2}(\sigma_h + t^2 \operatorname{Curl} \hat{\alpha}_h, \Pi_k \psi_h)_{L^2(\Omega)} - t^{-2}(\Pi_k \phi_h, \Pi_k \psi_h)_{L^2(\Omega)} \\ &\quad = (\Pi_k \eta, \Pi_k \psi_h)_{L^2(\Omega)}, \end{aligned}$$

which is the first equation of (4.7). For any $\beta_h \in Q_h$, the definition of $\hat{\alpha}_h$ and the orthogonality of σ_h to $\operatorname{Curl} Q_h$ imply

$$\begin{aligned} (\phi_h - t^2 \operatorname{Curl} \hat{\alpha}_h, \operatorname{Curl} \beta_h)_{L^2(\Omega)} &= (\sigma_h - t^2 \Pi_k \eta, \operatorname{Curl} \beta_h)_{L^2(\Omega)} \\ &= -t^2 (\eta, \operatorname{Curl} \beta_h)_{L^2(\Omega)}, \end{aligned}$$

which is the second equation of (4.7). This proves $\phi_h = \widetilde{\phi}_h$ and $\hat{\alpha}_h = \alpha_h$, and the definition of $\hat{\alpha}_h$ therefore implies (4.8). ∎

Remark 4.4. Since only standard finite element spaces are involved in system (4.7), it allows for a direct implementation. The classical FEMs of Arnold and Falk [5] and Durán and Liberman [18] have fewer degrees of freedom per element than $\Phi_h \times Q_h$. However, these methods are only of first order. The MITC7 finite element [9] is of second order but has 20 local degrees of freedom, while (4.7) for $k = 0$ has only 15 degrees of freedom per element and is also of second order.

4.3. Mixed system. This section rewrites problem (4.3) into a system of four equations. This splitting is a classical argument in the error analysis for finite elements for the Reissner–Mindlin plate, and it is used also in the error analysis in Theorem 5.5 below. For the continuous problem this splitting is well known [10] and stated in section 3. Note that $(f, s)_{L^2(\Omega)}$ in the right-hand side of (3.2a) can be replaced by $(\eta, \nabla s)_{L^2(\Omega)}$.

As in section 3, the discrete problem (4.3) can be reformulated as a mixed system: Seek $(\rho_h, \phi_h, p_h, \sigma_h) \in Z_h \times \Phi_h \times Q_h \times Z_h$ such that, for all $(\xi_h, \psi_h, q_h, \tau_h) \in Z_h \times \Phi_h \times Q_h \times Z_h$,

$$(\rho_h, \xi_h)_{L^2(\Omega)} = (\eta, \xi_h)_{L^2(\Omega)} \tag{4.9a}$$

$$a(\phi_h, \psi_h) - b(\psi_h, p_h) - (\rho_h, \psi_h)_{L^2(\Omega)} = 0 \tag{4.9b}$$

$$-b(\phi_h, q_h) - t^2 c(p_h, q_h) = 0 \tag{4.9c}$$

$$(\sigma_h, \tau_h)_{L^2(\Omega)} - (\phi_h, \tau_h)_{L^2(\Omega)} = t^2 (\eta, \tau_h)_{L^2(\Omega)}. \tag{4.9d}$$

The proof of the equivalence is based on introducing the discrete shear variable

$$\zeta_h = t^{-2} \Pi_k (\sigma_h - \phi_h) \tag{4.10}$$

and its discrete Helmholtz decomposition

$$\zeta_h = \rho_h + \operatorname{Curl} p_h \tag{4.11}$$

with $\rho_h \in Z_h$ and $p_h \in Q_h$ as discrete analoga of (1.2) and (1.3). The proof follows the lines of [21, Lemma 2] and is therefore skipped.

The definition of the shear variable (1.2) and the Helmholtz decomposition (1.3) show

$$\nabla r + \operatorname{Curl} p = t^{-2}(\nabla w - \phi).$$

TABLE 1
List of variables in the error analysis.

	Continuous	Discrete
Data	η with $-\operatorname{div}\eta = f$	$\Pi_k\eta$
Rotation	ϕ	ϕ_h
Displacement gr.	∇w	$\sigma_h \in Z_h$
Shear stress	$\zeta = t^{-2}(\nabla w - \phi)$	$\zeta_h = t^{-2}\Pi_k(\sigma_h - \phi_h)$
Helmholtz dec. 1	$\zeta = \nabla r + \operatorname{Curl} p$	$\zeta_h = \rho_h + \operatorname{Curl} p_h$
Helmholtz dec. 2	$\phi + t^2\eta = \nabla w + t^2 \operatorname{Curl}\alpha$	$\Pi_k(\phi_h + t^2\eta) = \sigma_h + t^2 \operatorname{Curl}\alpha_h$
Helmholtz dec. 3	$\eta = \nabla r + \operatorname{Curl}(\alpha + p)$	$\Pi_k\eta = \rho_h + \operatorname{Curl}(\alpha_h + p_h)$

This and (4.5) leads to

$$\eta = \nabla r + \operatorname{Curl}(\alpha + p). \tag{4.12}$$

Similarly, the corresponding discrete relations (4.10), (4.11), (4.8) lead to

$$\Pi_k\eta = \rho_h + \operatorname{Curl}(\alpha_h + p_h). \tag{4.13}$$

All relevant continuous and discrete variables and some of their relations are summarized in Table 1.

Since $Z_h \not\subseteq \nabla H^1_0(\Omega)$, (4.9) defines a nonconforming approximation of (3.2). However, the constraint from the definition of Z_h can be reformulated with the help of a Lagrange multiplier such that (4.9) results in a conforming system of six equations. The Helmholtz decompositions 2 and 3 from Table 1 show that the multipliers equal $p+\alpha$ for (3.2a) and $t^2\alpha$ for (3.2d). A preliminary error estimate can then be deduced using saddle-point theory. We mention the result here for completeness but do not comment on details because the bound is not optimal for our discretization.

PROPOSITION 4.5. *The error between the solutions to* (3.2) *and* (4.9),

$$\begin{aligned}&|\!|\!|\phi - \phi_h|\!|\!| + \|\nabla w - \sigma_h\| + \|p - p_h\| + t|p - p_h|_1\\ &\quad + \|\nabla r - \rho_h\| + |(p+\alpha) - (p_h + \alpha_h)|_1 + t^2|\alpha - \alpha_h|_1,\end{aligned}$$

is quasi-optimal.

As already mentioned, the polynomial degrees are chosen such that a term like $\|\nabla w - \sigma_h\|_{L^2(\Omega)}$ is generally approximated with a lower rate compared to $|\!|\!|\phi - \phi_h|\!|\!|$. Section 5 below derives error estimates which are balanced with respect to the approximation rates.

5. Error analysis. The first error estimate is based on the discretization of system (4.4).

PROPOSITION 5.1 (a priori error estimate). *Let ϕ and ϕ_h be the rotation parts of the solutions to* (1.1) *and* (4.3)*, respectively, and let α and α_h be as in* (4.4) *and* (4.7)*, respectively. It holds that*

$$\begin{aligned}&|\!|\!|\phi - \phi_h|\!|\!| + \|\alpha - \alpha_h\| + t|\alpha - \alpha_h|_1\\ &\quad\lesssim \inf_{\psi_h\in\Phi_h} |\!|\!|\phi - \psi_h|\!|\!| + \inf_{\beta_h\in Q_h}\big(\|\alpha - \beta_h\| + t|\alpha - \beta_h|_1\big) + \|h_{\mathcal{T}}(\eta - \Pi_k\eta)\|\end{aligned}$$

with a t-independent constant hidden in the notation $\lesssim$.

Proof. The result follows from the theory of saddle point problems with penalty term and a perturbation argument for the right-hand side. Let (ϕ_h', α_h') solve (4.7) where the right-hand side of the first equation is replaced by $(\eta, \psi_h)_{L^2(\Omega)}$. Then (ϕ_h', α_h') is a Galerkin approximation of (ϕ, α) from (4.4), and the theory [9] proves the quasi-best approximation property

$$\begin{aligned}&|||\phi - \phi_h'||| + \|\alpha - \alpha_h'\| + t|\alpha - \alpha_h'|_1 \\ &\quad \lesssim \inf_{\psi_h \in \Phi_h} |||\phi - \psi_h||| + \inf_{\beta_h \in Q_h} \big(\|\alpha - \beta_h\| + t|\alpha - \beta_h|_1\big).\end{aligned}$$

The global stability of the discrete system (4.7) shows that there exist $\psi_h \in \Phi_h$ and $\beta_h \in Q_h$ with norm $|||\psi_h||| + \|\beta_h\| + t|\beta_h|_1 \lesssim 1$ such that

$$\begin{aligned}&|||\phi_h - \phi_h'||| + \|\alpha_h - \alpha_h'\| + t|\alpha_h - \alpha_h'|_1 \\ &\quad \lesssim a(\phi_h - \phi_h', \psi_h) + b(\psi_h, \alpha_h - \alpha_h') + b(\phi_h - \phi_h', \beta_h) - t^2 c(\alpha_h - \alpha_h', \beta_h).\end{aligned}$$

By the discrete solution properties, the right-hand side of this estimate equals $(\Pi_k \eta - \eta, \psi_h)_{L^2(\Omega)}$ and can be estimated with a piecewise Poincaré inequality as follows:

$$(\Pi_k \eta - \eta, \psi_h)_{L^2(\Omega)} = (\Pi_k \eta - \eta, \psi_h - \Pi_0 \psi_h)_{L^2(\Omega)} \lesssim \|h_{\mathcal{T}}(\Pi_k \eta - \eta)\|_{L^2(\Omega)},$$

where the norm bound for $|\psi_h|_1 \lesssim |||\psi_h||| \lesssim 1$ has been used. The combination of the two error estimates with the triangle inequality proves the assertion. ∎

Remark 5.2. If $f \in H^m(\Omega)$ and η is obtained by integration, then $\eta \in H^{m+1}(\Omega)$ and the term $\|h_{\mathcal{T}}(\eta - \Pi_k \eta)\|$ converges with rate $O(h^{\min\{k+2, m+2\}})$.

Remark 5.3. If ϕ and α are sufficiently smooth, Proposition 5.1 and standard interpolation estimates lead to an asymptotic convergence rate of $\mathcal{O}(h^{k+2} + t h^{k+1})$ of the right-hand side of the error estimate with a multiplicative constant that involves higher-order (and generally t-dependent) derivatives of the solution. The terms in the upper bound are thus balanced when $t \lesssim h$. An estimate for the asymptotic regime $h \lesssim t$ will be given in Theorem 5.5.

Remark 5.4. The approximation error of the shear variable can be bounded with (4.6) and its discrete analogue as follows

$$\|\zeta - \zeta_h\|_{H^{-1}(\Omega)} \lesssim \|h_{\mathcal{T}}(\eta - \Pi_k \eta)\| + \|\alpha - \alpha_h\|.$$

If η, α, and ϕ are sufficiently smooth, Proposition 5.1 leads to a convergence rate of $\mathcal{O}(h^{k+2} + t h^{k+1})$ for the error of the shear variable in the $H^{-1}(\Omega)$ norm with a multiplicative t-dependent constant as in Remark 5.3.

Recall that $0 < s \leq 1$ denotes the elliptic regularity constant from the Poisson–Neumann problem (see (2.2)) and that $h = \max h_{\mathcal{T}}$ denotes the maximum mesh size.

THEOREM 5.5. *Let ϕ be the rotation part of the solution to* (1.1) *with α, p as in Table* 1. *The discrete solution $\phi_h \in \Phi_h$ of* (4.3) *satisfies*

$$\begin{aligned}|||\phi - \phi_h||| \lesssim{}& \inf_{\varphi_h \in \Phi_h} |||\phi - \varphi_h||| + h^s \inf_{q_h \in Q_h} |p - q_h|_1 \\ &+ h^s \inf_{\delta_h \in Q_h} |(\alpha + p) - \delta_h|_1 + \|h_{\mathcal{T}}(\eta - \Pi_k \eta)\|\end{aligned} \tag{5.1}$$

with a t-independent constant hidden in the notation $\lesssim$. In the classical language of asymptotic convergence rates, the following less sharp error bound is valid provided

that the variables are smooth enough (such that the right-hand side of the following expression is finite)

$$|||\phi - \phi_h||| \lesssim h^{k+2}\left(|\phi|_{k+3} + |\eta|_{k+1}\right) + h^{k+s+1}\left(|\alpha + p|_{k+2} + |p|_{k+2}\right). \tag{5.2}$$

Proof. The proof follows similar as the proof of Theorem 3.1 so that only the differences are highlighted here.

The estimate

$$\begin{aligned} |||\phi - \phi_h|||^2 \lesssim \inf_{\varphi_h \in \Phi_h} |||\phi - \varphi_h|||^2 + h^s \inf_{s_h \in Q_h} |p - s_h|_1^2 \\ + (\nabla r - \rho_h, \psi_h - \phi_h)_{L^2(\Omega)} \end{aligned} \tag{5.3}$$

follows exactly as in step 1 of the proof of Theorem 3.1 except that $\nabla_{\mathrm{NC}} r_{\mathrm{CR}}$ is replaced by ρ_h. For $\gamma := \alpha + p \in Q$ and $\gamma_h := \alpha_h + p_h \in Q_h$, Table 1 shows the Helmholtz decompositions

$$\eta = \nabla r + \operatorname{Curl} \gamma \qquad \text{and} \qquad \Pi_k \eta = \rho_h + \operatorname{Curl} \gamma_h.$$

With this, the proof of Theorem 5.5 follows the lines of step 3 of Theorem 3.1 with $\nabla_{\mathrm{NC}} r_{\mathrm{CR}}$ replaced by ρ_h and $\Pi_0 \eta$ replaced by $\Pi_k \eta$. ∎

Remark 5.6. The norm of $\alpha + p$ on the right-hand side of (5.1)–(5.2) in Theorem 5.5 is independent of t because $\alpha + p$ stems from a Helmholtz decomposition of the data η; see Table 1. The norm of p is estimated via the relations of Table 1 as $|p|_{k+2} \leq |\zeta|_{k+1} + |r|_{k+2}$, where r solves the Poisson equation with right-hand side f and is therefore independent of t.

The combination of Proposition 5.1 and Theorem 5.5 leads to the following error estimate.

COROLLARY 5.7. *Let ϕ be the rotation part of the solution to* (1.1) *with α, p as in Table* 1. *The discrete solution $\phi_h \in \Phi_h$ of* (4.3) *satisfies*

$$\begin{aligned} |||\phi - \phi_h||| \lesssim \inf_{\psi_h \in \Phi_h} |||\phi - \psi_h||| + \|h_{\mathcal{T}}(\eta - \Pi_k \eta)\| \\ + \min\Big\{ h^s \inf_{q_h \in Q_h} |p - q_h|_1 + h^s \inf_{\delta_h \in Q_h} |(\alpha + p) - \delta_h|_1, \\ \inf_{\beta_h \in Q_h} \left(\|\alpha - \beta_h\| + t|\alpha - \beta_h|_1 \right) \Big\} \end{aligned}$$

with a t-independent constant hidden in the notation $\lesssim$. In terms of asymptotic convergence rates, the approximation is of the order

$$h^{k+2}(|\phi|_{k+3} + |\eta|_{k+1}) + \min\{h^{k+1+s}(|p|_{k+2} + |\alpha + p|_{k+2}), (h+t)h^{k+1}|\alpha|_{k+2}\}.$$

6. Numerical results. This section illustrates the behavior of the new method in numerical experiments.

6.1. Experiment 1: Convergence rates on the square domain. The underlying domain is the unit square $\Omega = (0,1)^2$ and the exact solution from [15] is given by

$$\phi(x,y) = \begin{bmatrix} y^3(y-1)^3x^2(x-1)^2(2x-1) \\ x^3(x-1)^3y^2(y-1)^2(2y-1) \end{bmatrix}$$

and

$$w(x,y) = \frac{1}{3}x^3(x-1)^3y^3(y-1)^3 - \frac{2t^2}{5(1-\nu)}\Big[y^3(y-1)^3x(x-1)(5x^2-5x+1) + x^3(x-1)^3y(y-1)(5y^2-5y+1)\Big].$$

The right-hand side $f(x,y)$ of (1.1) is given by $E/(12(1-\nu^2))$ times

$$\Big[12y(y-1)(5x^2-5x+1)\Big(2y^2(y-1)^2 + x(x-1)(5y^2-5y+1)\Big) + 12x(x-1)(5y^2-5y+1)\Big(2x^2(x-1)^2 + y(y-1)(5x^2-5x+1)\Big)\Big].$$

The material parameters read $\nu = 0.3$, $E = 10^6$, and $\kappa = 5/6$, while the two values $\tilde{t} = 0.1$ and $\tilde{t} = 0.01$ are chosen for the plate thickness (recall the relationship of t and $\tilde{t}$ from section 2). In this case, the field η with $-\operatorname{div}\eta = f$ is obtained by explicit integration of the polynomial f: The first summand is integrated with respect to x and the second one with respect to y to build the components $-\eta_1$, $-\eta_2$.

We approximate the problem on uniformly refined meshes of mesh size $h \in \sqrt{2} \times \{2^{-1}, \dots, 2^{-6}\}$ for polynomial degrees $k = 0, 1, 2$. The relative errors

$$e(\phi) := \frac{|\phi - \phi_h|_1}{|\phi|_1} \quad \text{and} \quad e(w) := \frac{\|\nabla w - \sigma_h\|_{L^2(\Omega)}}{\|\nabla w\|_{L^2(\Omega)}}$$

are displayed in Figure 1. The approximation of ∇w is observed to converge at rate h^{k+1} while ϕ is approximated with the higher rate h^{k+2}. The errors for the two values of t are of similar size. The computations indicate that all variables have the necessary smoothness properties so that the predicted approximation properties from section 5 result in the full asymptotic convergence rates.

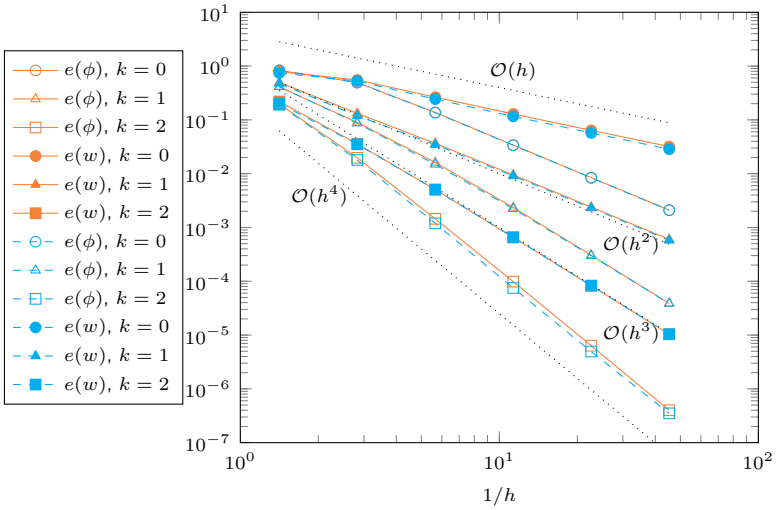

FIG. 1. *Experiment 1: Convergence history for ϕ and ∇w with $k = 0, 1, 2$ for $\tilde{t} = 0.1$ (solid lines) and $\tilde{t} = 0.01$ (dashed lines).*

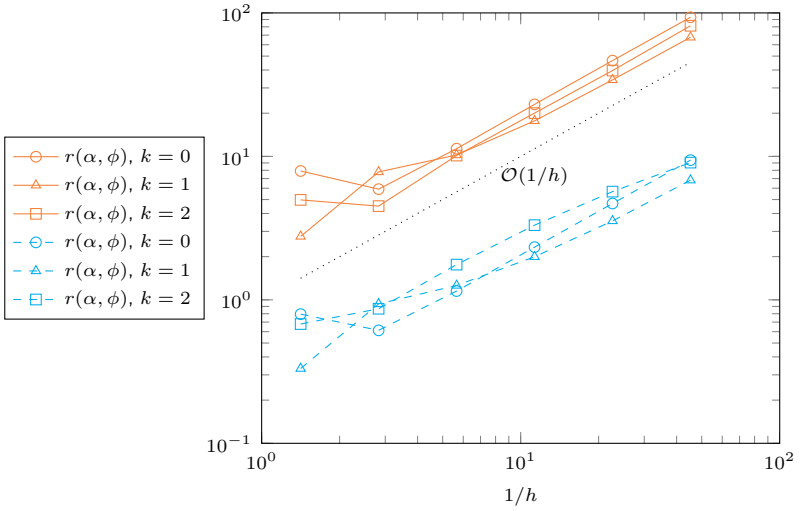

FIG. 2. *Experiment* 1*: The ratio* $r(\alpha,\phi) = t|\alpha-\alpha_h|_1/|\phi-\phi_h|_1$ *with* $k=0,1,2$ *for* $\tilde{t}=0.1$ *(solid lines) and* $\tilde{t}=0.01$ *(dashed lines).*

In order to illustrate the preasymptotic and the asymptotic aspects of the a priori error analysis, we consider the ratio

$$r(\alpha,\phi) := \frac{t|\alpha-\alpha_h|_1}{|\phi-\phi_h|_1}.$$

An exact expression for α is not known, but the error $t|\alpha-\alpha_h|_1$ can be approximated as follows. Elementary algebraic manipulations, the Helmholtz decomposition 2 from Table 1, and the L^2 orthogonality of $\nabla w - \sigma_h$ on $\operatorname{Curl}\alpha_h$ prove the identity

$$t^2|\alpha-\alpha_h|_1^2 = t^2|\alpha|_1^2 - t^2|\alpha_h|_1^2 + 2(\phi_h-\phi,\operatorname{Curl}\alpha_h)_{L^2(\Omega)}.$$

Since α is the solution to the Neumann problem $-\Delta\alpha = \operatorname{rot}(t^{-2}\phi+\eta)$ and the right-hand side is known, an approximation for $|\alpha|_1$ can be obtained by solving a discrete Neumann problem with a higher-order method, and this approximation can be used to compute the right-hand side of the above formula. The reference values $|\alpha|_1 = 2.363277353903799$ for $\tilde{t}=0.1$ and $|\alpha|_1 = 2.363277353902728$ for $\tilde{t}=0.01$ were obtained by a quartic FEM on a uniform mesh with mesh size $h=2^{-8}\sqrt{2}$. The ratio $r(\alpha,\phi)$ is displayed in Figure 2. On fine meshes the ratio diverges under mesh refinement. This is the asymptotic regime where the higher-order approximation of ϕ is explained by Theorem 5.5. For small $\tilde{t}=0.01$ and coarse meshes, the ratio is small. This is the regime where the right-hand side of Proposition 5.1 guarantees accuracy for the approximation of ϕ.

6.2. Experiment 2: Locking test with the biharmonic equation. This test is devoted to an illustration of the locking-free error estimates of this paper. The domain Ω is the square $\Omega=(0,\pi)^2$. The exact solution of the biharmonic equation is given by $w(x,y)=\sin^2(x)\sin^2(y)$, $\phi=\nabla w$, and $f=\frac{E}{12(1-\nu^2)}\Delta^2 w$, where the material parameters are taken as $E=1000$, $\nu=0.3$, $\kappa=5/6$. The right-hand side η is chosen as $\eta=(-F,0)$ with the antiderivative F of f with respect to x. The numerical scheme for the Reissner–Mindlin plate is expected to deliver accurate approximations to this

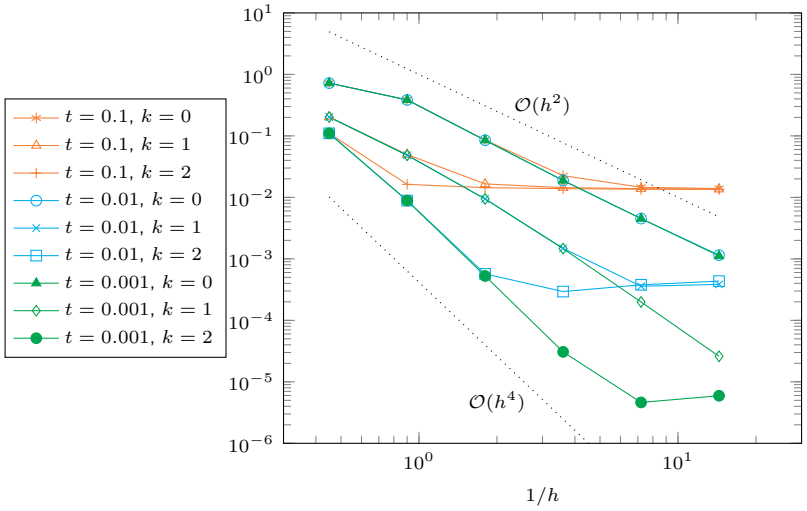

FIG. 3. *Experiment 2: Convergence history of the relative error $e(\phi)$ for $\tilde{t} = 0.1$, $\tilde{t} = 0.01$, $\tilde{t} = 0.001$.*

solution as long as t is small compared to h. Figure 3 displays the convergence history of the ϕ variable for the discretization parameters $k = 0, 1, 2$ and thickness parameters $\tilde{t} = 0.1$, $\tilde{t} = 0.01$, $\tilde{t} = 0.001$. Preasymptotically, optimal-in-h convergence and the robustness with respect to t can be observed. The errors are, as expected, bounded from below by the model error between the two plate models.

6.3. Experiment 3: Solution with thickness-dependent rotation. In contrast to the first test of section 6.1, where convergence rates are illustrated but the dependance on the thickness t is uncritical, this experiment is concerned with a setting where the exact solution shows the generic t-dependent growth of higher-order Sobolev norms [6]. The only known exact solution of this type that we are aware of was provided by [4] for the unit disc $\Omega = \{x^2 + y^2 < 1\}$. In order to stay in the setting where our proofs apply, we choose polygonal approximations from the interior. It is known that approximating the disc with polygons slows down the order of convergence [9], but a rate of $h^{3/2}$ can be expected when quadratic approximations are used. This applies to the classical Taylor–Hood pairing, so that in the lowest-order case $k = 0$ a comparison with the Mini element (the original method of [5]), which is first-order in h, is possible. In order to make t-dependent effects visible in this situation, we need to choose a setting where the H^s norm of ϕ with $2 \le s \le 3$ deteriorates with t, and this is the case for the soft simply-supported boundary condition, which imposes the condition $w = 0$ on $\partial\Omega$ and no essential boundary condition on ϕ. The exact solution from [4, Table 4] is given in polar coordinates (r, θ) as follows. Given the material parameters E, ν, κ, and the (scaled) thickness parameter t, define the constants

$$\lambda = (1+\nu)^{-1} E\kappa/2, \quad \tilde{t} = \lambda^{1/2} t, \quad \mathbb{D} = E/(12(1-\nu^2)), \quad \boldsymbol{\alpha} = \sqrt{12\kappa},$$

where $\tilde{t}$ refers to the physical plate thickness as in earlier sections. Given the right-hand side $f(r, \theta) = \cos\theta$, the rotation ϕ (given in radial and angular parts) and the displacement w read

$$\phi_r = [4r^3/(45\mathbb{D}) + 3\boldsymbol{a}r^2 + \boldsymbol{b} - \boldsymbol{c}\lambda^{-1}\tilde{t}^2 + r^{-1}\lambda^{-1}\boldsymbol{d}\tilde{t}^2 I_1(\boldsymbol{\alpha}r/\tilde{t})]\cos\theta$$
$$\phi_\theta = [-r^3/(45\mathbb{D}) - \boldsymbol{a}r^2 - \boldsymbol{b} + \boldsymbol{c}\lambda^{-1}\tilde{t} - \boldsymbol{d}\boldsymbol{\alpha}\lambda^{-1}\tilde{t}I_1'(\boldsymbol{\alpha}r/\tilde{t})]\sin\theta$$
$$w = [r^4/(45\mathbb{D}) - \lambda^{-1}\tilde{t}^2 r^2/3 + \boldsymbol{a}(r^3 - 8\mathbb{D}\lambda^{-1}r\tilde{t}^2) + \boldsymbol{b}r - \boldsymbol{c}\lambda^{-1}\tilde{t}^2 r]\cos\theta.$$

Here, I_1 is the modified Bessel function of the first kind [1] of order 1, and the functions involved in these expressions are given as follows:

$$\boldsymbol{f} = 15[(3\boldsymbol{\alpha}^2 + \boldsymbol{\alpha}^2\nu + 8\tilde{t}^2)I_1(\boldsymbol{\alpha}/\tilde{t}) - 8\boldsymbol{\alpha}\tilde{t}I_1'(\boldsymbol{\alpha}/\tilde{t})],$$
$$\boldsymbol{a} = [-(4\boldsymbol{\alpha}^2 + \boldsymbol{\alpha}^2\nu + 10\tilde{t}^2)I_1(\boldsymbol{\alpha}/\tilde{t}) + 10\boldsymbol{\alpha}\tilde{t}I'(\boldsymbol{\alpha}/\tilde{t})]/(2\mathbb{D}\boldsymbol{f}), \quad \boldsymbol{c} = \boldsymbol{\alpha}^2(1-\nu)I_1(\boldsymbol{\alpha}/\tilde{t})/\boldsymbol{f},$$
$$\boldsymbol{b} = [(6\boldsymbol{\alpha}^2 + \boldsymbol{\alpha}^2\nu + 14\tilde{t}^2)I_1(\boldsymbol{\alpha}/\tilde{t}) - 14\boldsymbol{\alpha}\tilde{t}I_1'(\boldsymbol{\alpha}/\tilde{t})]/(6\mathbb{D}\boldsymbol{f}), \quad \boldsymbol{d} = 2\lambda/(\mathbb{D}\boldsymbol{f}).$$

We choose the material parameters as $E = 1$, $\nu = 0.3$, $\kappa = 5/6$ and note that $\eta(r,\theta) = r\binom{\sin^2(\theta)}{-\sin(\theta)\cos(\theta)}$ satisfies $-\operatorname{div}\eta = f$. We compare two choices of mesh refinement. The first variant is uniform mesh refinement where, after refinement, the resulting boundary vertices are projected to the boundary $\partial\Omega$. The second variant combines the same uniform refinement rule with one local refinement of all elements near the boundary after each step. The precise rule we use is to mark all triangles containing a boundary vertex, to refine according to newest-vertex bisection [26], and to project new boundary points to the boundary of Ω. In all diagrams, the symbol h refers to the maximal mesh size, so that the locally refined meshes have a resolution of order h^2 near the boundary.

Figure 4 shows the convergence history of the relative errors in the ϕ variable with $k = 0, 1, 2$ and thickness $\tilde{t} = 1$. For this moderate value, the asymptotic convergence rates can be observed starting from the first mesh for $k = 1, 2$, while for $k = 0$, a pre-asymptotic convergence rate of h^2 is observed. Uniform mesh refinement yields sub-optimal rates due to the polygonal approximation, while the local refinement strategy leads to optimal rates up to the order h^3. For $k = 2$, where quartic elements are used, the optimal rate h^4 would require further resolution of the curved boundary, which

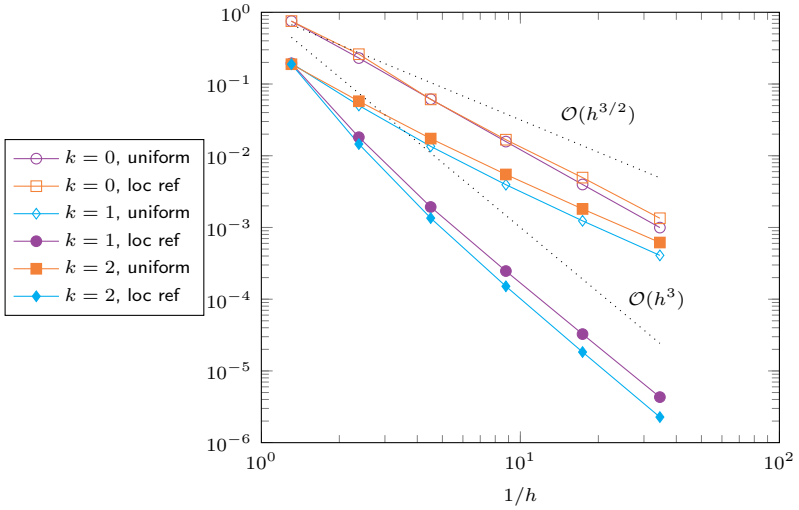

FIG. 4. *Experiment 3: Convergence history for ϕ with $\tilde{t} = 1$ and $k = 0, 1, 2$ with uniform mesh refinement (uniform) and on meshes adapted to the boundary (loc ref).*

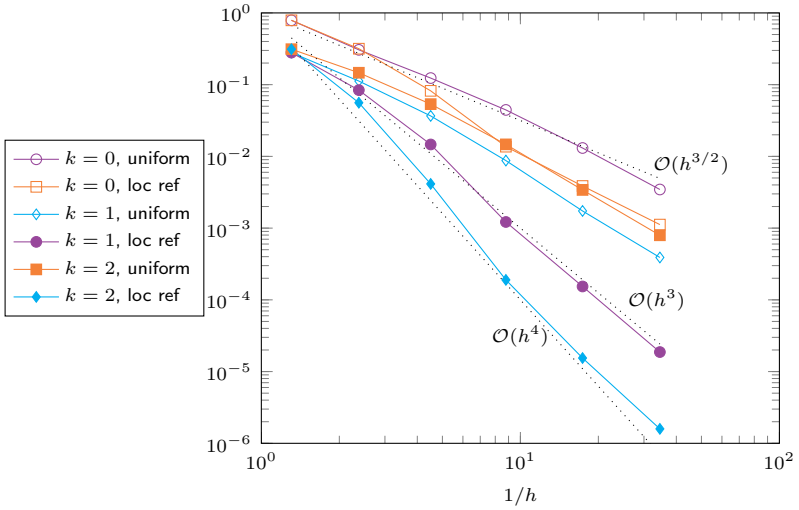

FIG. 5. *Experiment 3: Convergence history for ϕ with $\tilde{t} = 0.1$ and $k = 0, 1, 2$ with uniform mesh refinement (uniform) and on meshes adapted to the boundary (loc ref).*

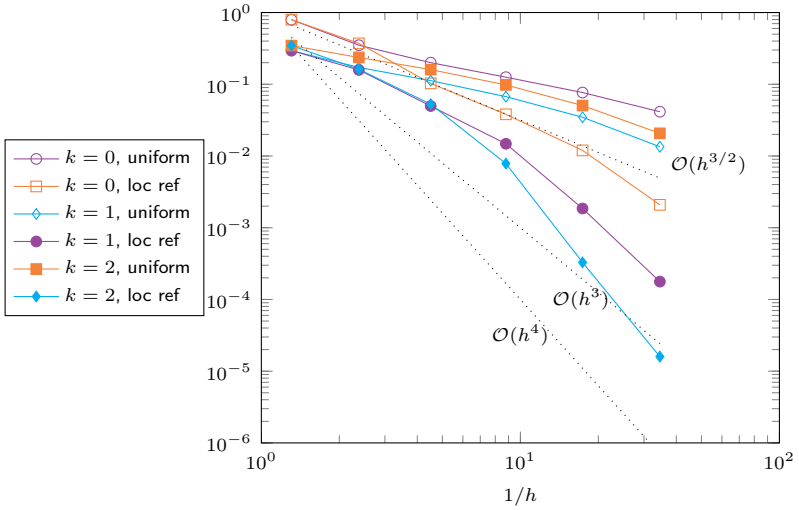

FIG. 6. *Experiment 3: Convergence history for ϕ with $\tilde{t} = 0.01$ and $k = 0, 1, 2$ with uniform mesh refinement (uniform) and on meshes adapted to the boundary (loc ref).*

we do not consider here because the focus is on the dependence on the parameter $\tilde{t}$ rather than h. Figure 5 shows the relative errors in the ϕ variable for $\tilde{t} = 0.1$. The same asymptotic rates can be observed in this example. For uniform meshes they are visible after two refinements while for the boundary-adapted strategy they are observable after the first refinement. Figure 6 shows the relative errors in the ϕ variable for $\tilde{t} = 0.01$. After the third refinement (that is, $h \sim 1/10$ and thus a mesh size of about $1/100$ near the boundary), the locally adapted meshes yield the asymptotic (or even pre-asymptotically better) rates, while for uniform meshes at least four refinements are needed to reach the optimal rate of $O(h^{3/2})$, which still seem insufficient for the asymptotic rate in the case $k = 0$.

It can be observed that preasymptotically the approximation deteriorates with small t, which is explained by the scaling of the H^3 norm on the right-hand side of the estimate of Theorem 5.5. This effect is not related to locking but to the t-dependent scaling of the PDE solution, and it can be mitigated (as shown in the numerical experiment) by locally resolving the boundary layer. Once the boundary layer of the solution is resolved by the mesh, optimal convergence rates can be observed. We mention that an anisotropic a priori grading seems to be most appropriate, but we disregard this option here because it is beyond the scope of this paper. The same applies to a posteriori error analysis (which would require a generalization of [12]) and automatic mesh-adaptation strategies.

REFERENCES

[1] M. Abramowitz and I. A. Stegun, *Handbook of Mathematical Functions with Formulas, Graphs, and Mathematical Tables*, National Bureau of Standards Applied Mathematics Series 55, Washington, D.C., 1964.

[2] D. N. Arnold and F. Brezzi, *Mixed and nonconforming finite element methods: Implementation, postprocessing and error estimates*, RAIRO Modél. Math. Anal. Numér., 19 (1985), pp. 7–32.

[3] D. N. Arnold, F. Brezzi, and M. Fortin, *A stable finite element for the Stokes equations*, Calcolo, 21 (1984), pp. 337–344 (1985).

[4] D. N. Arnold and R. S. Falk, *Edge Effects in the Reissner-Mindlin Plate Theory*, in Analytic and Computational Models of Shells, A. K. Noor, T. Belytschhko, and J. Simo, eds., A.S.M.E., New York, 1989, pp. 71–90.

[5] D. N. Arnold and R. S. Falk, *A uniformly accurate finite element method for the Reissner-Mindlin plate*, SIAM J. Numer. Anal., 26 (1989), pp. 1276–1290.

[6] D. N. Arnold and R. S. Falk, *The boundary layer for the Reissner-Mindlin plate model*, SIAM J. Math. Anal., 21 (1990), pp. 281–312.

[7] D. Boffi, *Stability of higher order triangular Hood-Taylor methods for the stationary Stokes equations*, Math. Models Methods Appl. Sci., 4 (1994), pp. 223–235.

[8] D. Boffi, F. Brezzi, and M. Fortin, *Mixed Finite Element Methods and Applications*, Springer Series in Computational Mathematics 44, Springer, Heidelberg, 2013.

[9] D. Braess, *Finite Elements. Theory, Fast Solvers, and Applications in Elasticity Theory*, 3rd ed., Cambridge University Press, Cambridge, UK, 2007.

[10] F. Brezzi and M. Fortin, *Numerical approximation of Mindlin-Reissner plates*, Math. Comp., 47 (1986), pp. 151–158.

[11] F. Brezzi, M. Fortin, and R. Stenberg, *Error analysis of mixed-interpolated elements for Reissner-Mindlin plates*, Math. Models Methods Appl. Sci., 1 (1991), pp. 125–151.

[12] C. Carstensen, *Residual-based a posteriori error estimate for a nonconforming Reissner-Mindlin plate finite element*, SIAM J. Numer. Anal., 39 (2002), pp. 2034–2044.

[13] C. Carstensen, D. Gallistl, and M. Schedensack, *Adaptive nonconforming Crouzeix-Raviart FEM for eigenvalue problems*, Math. Comp., 84 (2015), pp. 1061–1087.

[14] C. Carstensen, D. Peterseim, and M. Schedensack, *Comparison results of finite element methods for the Poisson model problem*, SIAM J. Numer. Anal., 50 (2012), pp. 2803–2823.

[15] C. Chinosi and C. Lovadina, *Numerical analysis of some mixed finite element methods for Reissner–Mindlin plates*, Comput. Mech., 16 (1995), pp. 36–44.

[16] M. Crouzeix and R. S. Falk, *Nonconforming finite elements for the Stokes problem*, Math. Comp., 52 (1989), pp. 437–456.

[17] E. Dari, R. Duran, C. Padra, and V. Vampa, *A posteriori error estimators for nonconforming finite element methods*, RAIRO Modél. Math. Anal. Numér., 30 (1996), pp. 385–400.

[18] R. Durán and E. Liberman, *On mixed finite element methods for the Reissner-Mindlin plate model*, Math. Comp., 58 (1992), pp. 561–573.

[19] R. S. Falk, *A Fortin operator for two-dimensional Taylor-Hood elements*, ESAIM, Math. Model. Numer. Anal., 42 (2008), pp. 411–424.

[20] M. Fortin and M. Soulie, *A nonconforming piecewise quadratic finite element on triangles*, Internat. J. Numer. Methods Engrg., 19 (1983), pp. 505–520.

[21] D. Gallistl and M. Schedensack, *A robust discretization of the Reissner–Mindlin plate with arbitrary polynomial degree*, J. Comput. Math., 38 (2020), pp. 1–13.

[22] P. Grisvard, *Singularities in Boundary Value Problems*, Recherches en Mathématiques Appliquées 22, Masson, Paris, 1992.
[23] T. Gudi, *A new error analysis for discontinuous finite element methods for linear elliptic problems*, Math. Comp., 79 (2010), pp. 2169–2189.
[24] M. Schedensack, *A new generalization of the P_1 non-conforming FEM to higher polynomial degrees*, Comput. Methods Appl. Math., 17 (2017), pp. 161–185.
[25] A. Veeser and P. Zanotti, *Quasi-optimal nonconforming methods for symmetric elliptic problems.* II—*Overconsistency and classical nonconforming elements*, SIAM J. Numer. Anal., 57 (2019), pp. 266–292.
[26] R. Verfürth, *A Posteriori Error Estimation Techniques for Finite Element Methods*, Numerical Mathematics and Scientific Computation, Oxford University Press, Oxford, 2013.